Unconventional Plasmons Induced by Electron Confinement and Strong Coulomb Correlations in $SrNbO_{3+\delta}$ family

M. A. Majidi,[1] W. Wilwin,[1] Andes R. P. Tambunan,[1] and Andrivo Rusydi[2,3,4]

[1] *Departemen Fisika, FMIPA, Universitas Indonesia, Depok 16424, Indonesia*
[2] *Singapore Synchrotron Light Source (SSLS), National University of Singapore, 5 Research Link, Singapore 117603, Singapore*
[3] *NUSSNI-NanoCore, National University of Singapore, Singapore 117576, Singapore*
[4] *Department of Physics, National University of Singapore, Singapore 117542, Singapore*

(Dated: March 5, 2019)

Recent experimental study revealed a new kind of plasmons in the Mott-insulating-like phase of thin film samples from $SrNbO_{3+\delta}$ family. These unconventional plasmons have been attributed to the interplay between electron confinement due to extra oxygen planes and electronic correlations. Attempts to explain the phenomenon have also been proposed at the level of classical coupled-oscillators model and ab-initio calculations, giving rise to results that resemble the experimental optical and plasmonic spectra. In this letter, we propose a more microscopic and quantum mechanical approach to explain the occurrence of such correlated plasmons. Our calculations excellently reproduce the frequency-dependent behavior of the experimental optical and plasmonic spectra of both the metallic- and the Mott-insulating-like phases. Our results validate some previous findings and provide a deeper physical insight into the mechanism of unconventional plasmons generation.

Plasmonics ability to confine and manipulate light in nanometre length scale enables technologies with unprecedented level of synergy between high-bandwidth capability of photonics and nanoscale integrability of nanoelectronics, forming the basis of a new research area called nanophotonics [1–7]. Plasmonics utilizes plasmon, a collective excitation that arise from interaction between electromagnetic fields and charges in solids. There are at least three known types of plasmons: conventional bulk (volume) plasmons, surface plasmons (SP), and localized surface plasmons (LSP). The first type is characterized by longitudinal oscillations accompanied by compressions of the electron gas in solids [8–11], the second type propagates transversal and strongly confined to the surface [12–14], and the last type is resulted from the confinement of SP in nanoparticles [15, 16]. However, it has been theoretically proven that a new kind of plasmons with multiple plasma frequencies can be generated by considering Coulomb interactions between charges in insulating phase of strongly correlated system [17]. This kind of plasmons are called correlated plasmons, because it arises from collective excitation of correlated electrons.

The first experimental work on the generation of correlated plasmons [18] shows that the insulating phase of Strontium Niobate Oxide under oxygen enrichment ($Sr_{1-x}NbO_{3+\delta}$) can have multiple low-loss plasmons formation in the visible-ultraviolet range. According to their hypotesis, the emergence of these plasmons are because of the presence of extra oxygen planes in $Sr_{1-x}NbO_{3+\delta}$ which changes the itinerant behaviour of the Nb-4d electrons into localized. This extra oxygen planes turn the system from a weakly-correlated conductor into a strongly-correlated Mott-like insulator.

Along with the experimental data, theoretical attempts to explain the occurence of such correlated plasmons in $SrNbO_{3+\delta}$ have also been proposed. A semi-classical and phenomenological approach in Ref. [18] through a seven coupled-oscillators model which is capable to reproduce qualitatively the optical and plasmonics spectra of the experimental data. These convenient result between experimental and theoretical approach suggest that the confinement of electrons due to extra oxygen planes along with electron-electron Coulomb interaction induces correlation effects that transform the previously three-dimensional itinerant electron system to a quasi-one-dimensional coupled-oscillators system with the masses and charges being renormalized in some way. However, it remains to be clarified as how such a transformation or renormalization arises quantum mechanically. Another approach is using density functional theory (DFT) with random phase approximation (RPA) by taking the local field effects (LFE) into account [19]. The results show several correlated plasmons although the plasmons occurence frequencies and amplitudes do not precisely match the experimental result in [18]. Therefore, in this letter, we propose a more microscopic and quantum mechanical model to provide a more physically insightful explanation of the occurring phenomenon.

Our model is based on the structure of $SrNbO_{3+\delta}$ synthesized at high oxygen pressure (hp-SNO) in Ref.[18]. The hp-SNO shows similar short-range perovskite structure interspersed with high density oxygen planes as the known structure of $SrNbO_{3,4}$. This extra oxygen planes caused by the oxygen enrichment occurs every five NbO_6 octahedrals aligned along [011]. By assuming that the electrons hopping are only take place between the nearest-neighbors Nb sites, we found that the most effective model is a 1D finite-size model as shown in Fig.1. The electronic states of strontium and oxygen atoms are not included in our model because previous calculation using DFT shows that the state at the Fermi energy of $SrNbO_{3,4}$ mainly comes from Nb-4d electrons [22, 23] es-

pecially electrons on the middle of NbO_6 sites. This size reduction and also the alignment of NbO_6 are then justify us to build a Hamiltonian of 1D finite-size modified Hubbard model around quarter-filling as:

$$\hat{H} = \sum_i \epsilon_i a^\dagger_{i\sigma} a_{i\sigma} - t \sum_{<ij>} a^\dagger_{i\sigma} a_{j\sigma} + U \sum_i \hat{n}_{i\uparrow}\hat{n}_{i\downarrow} + V \sum_{\substack{<ij> \\ \sigma,\sigma'}} \hat{n}_{i\sigma}\hat{n}_{j\sigma'} \quad (1)$$

where ϵ_i denotes the on-site energy at site i, t denotes the hopping amplitude, U denotes the on-site Coulomb repulsion parameter, and V denotes nearest neighbours inter-site Coulomb repulsion.

The first term in Eq. (1) is used to model the differences in Coulomb potential energy experienced by the outermost sites (nearest to the extra oxygen planes), second outermost sites, and the middle site. Using a simple electrostatic potential energy formula, we obtain that the outermost sites and second outermost sites, respectively, have energy $11zke^2/12a$ and $zke^2/6a$ relative to the middle site, with k refers to Coulomb constant, z to the ion's charge number, a to the system's lattice constant, and e to the electron's charge. By this calculation, we obtain an ideal ratio between the outermost on-site energy with the second outermost on-site energy is $11:2$.

The second and the third term together are the Hubbard Hamiltonian. The second term models the effective electron hopping between Nb atoms, and the third term models the on-site Coulomb repulsion if there is a doubly occupied site.

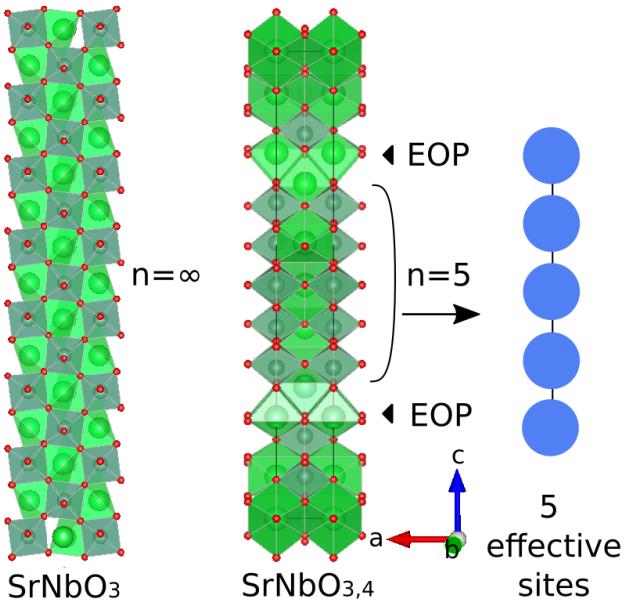

FIG. 1: The crystal structure of stoichiometric $SrNbO_3$ and $SrNbO_{3,4}$ (structural data is taken from Ref.[20, 21]). The ilustration of 1D finite-size chain. Blue circles represent the effective Nb sites.

Regarding the main aim of this letter is to mimic the experimental result of hp-SNO shown in [18], it is necessary to construct a model which can be tuned into an insulator. For a system that is far from half-filling, Hubbard-U is insufficient to turn the system into an insulator, thus we have to include the long-range Coulomb repulsions. This might prove the hypothesis that the long-range Coulomb interactions are not screened in hp-SNO. To model the long-range Coulomb repulsions we use only nearest-neighbor intersite Coulomb repulsions denoted by V and assume that other intersite terms that is farther away from the nearest neighbor are negligible.

For the 1D finite-size modified Hubbard model, we obtain the eigenenergies and eigenstates for N-particle Hamiltonian matrix by using exact-diagonalization method. Afterward, by the resulting eigenenergies and eigenstates, we construct the corresponding single-particle retarded Green's function at zero temperature by means of Lehmann's representation as below:

$$G^R_{\alpha\beta}(\omega) = \sum_n \left[\frac{\langle \Psi^N_0 | c_\alpha | \Psi^{N+1}_n \rangle \langle \Psi^{N+1}_n | c^\dagger_\beta | \Psi^N_0 \rangle}{\omega - (E^{N+1}_n - E^N_0) + i\eta} \right] + \sum_m \left[\frac{\langle \Psi^N_0 | c^\dagger_\beta | \Psi^{N-1}_m \rangle \langle \Psi^{N-1}_m | c_\alpha | \Psi^N_0 \rangle}{\omega + (E^{N-1}_m - E^N_0) + i\eta} \right]. \quad (2)$$

In this equation, α and β are indicating the site-spin coordinates of the initial and the final state of an electron, Ψ^N_0 is the ground state of N particles system, and $\Psi^{N\pm1}_n$ is the states of $N \pm 1$ particles system, which all of them have already obtained by using the exact-diagonalization method. The Lehmann's representation in Eq.(2) is a canonical ensemble average Green's function as we only allow the particles to fluctuate between $N-1$ and $N+1$ where the average number of particle N is constant. So now we can calculate the optical conductivity as also previously used in [24–26] using:

$$Re\sigma(\omega) = \frac{1}{N_{sites}} \frac{\pi e^2}{\hbar a} \int_{\mu-\omega}^{\mu} d\nu \left(\frac{f(\nu,\mu,T) - f(\nu+\omega,\mu,T)}{\omega} \right) \times Tr\left[v_{\alpha\beta}\right]\left[A_{\alpha\beta}(\nu)\right]\left[v_{\alpha\beta}\right]\left[A_{\alpha\beta}(\nu+\omega)\right], \quad (3)$$

where the velocity matrix defined as $v_{j,\sigma,j\pm1,\sigma'} = \pm it$ and zero elsewhere as only nearest neighbor hopping is considered, j denotes the site of the one dimensional finite-size model, and $A_{\alpha\beta}(\nu)$ denotes the spectral function obtained from Eq.(2). We set $T = 0$ in our calculations as we only interested in the ground-state properties of the system. Next we use the Kramers-Kronig relation to produce the imaginary part so we obtain the complex equation of $\sigma(\omega)$.

We use the conductivity-permitivity relationship in order to obtain the real and imaginary parts of the complex dielectric functions: Finally, we calculate the loss function (LF) of the system by using $LF(\omega) = -Im[\varepsilon^{-1}]$,

where ε denotes the complex dielectric function. This is a property that measure the absorbance of system towards energy received from external perturbation in form of electron-electron perturbation, which for plasmonics case this property is the most important quantity obtained from Electron Energy Loss Spectroscopy (EELS).

Beside of the 1D model, here we also present a additional model which is constructed from a 3D bulk system. This model is proposed to be a comparation to the preceding model. By this model we emphasize the importance of confinement in the generation of correlated plasmons. The Hamiltonian of this model is expressed as:

$$\begin{aligned}\hat{H} = &\sum_{\vec{k},\alpha,\beta,\sigma} \epsilon_{\vec{k}} c^{\dagger}_{\vec{k}\alpha\sigma} c_{\vec{k}\beta\sigma} + U \sum_{\alpha\sigma} \hat{n}_{\alpha\sigma} \langle \hat{n}_{\alpha\bar{\sigma}} \rangle \\ &+ V \sum_{\alpha,\beta,\sigma} \hat{n}_{\alpha\sigma} \big(\langle \hat{n}_{\beta\uparrow} \rangle + \langle \hat{n}_{\beta\downarrow} \rangle \big)\end{aligned} \tag{4}$$

with $\epsilon_{\vec{k}} = -2t\,(\cos k_x a + \cos k_y a + \cos k_z a)$ is a tight-binding dispersion relation, α and β are indices for neighboring sublattices, and σ refers to the electron's spin. We later note that in the 3D model, the variation of V will only shift the system's density of states (DOS) and chemical potential (μ) by a constant factor, so this parameter will not affect the results.

We treat the 3D model in Eq.(4) using a self-consistent Green's function within mean-field theory and Kubo formula to obtain the real part of optical conductivity. Here, we are only interested in the longitudinal component of optical conductivity and the ground-state properties ($T = 0$) of the 3D system. Then we obtain the other optical properties of this model using the same method as previously used in the 1D model.

We are now moving to the discussion of 1D model calculation's results. We vary several parameters such as the number of sites (N), number of electrons (N_E), hopping parameter, on-site and inter-site Coulomb repulsion, and also on-site energy to find the set of parameters that can best fit the experimental data. Especially for variable ϵ_i, the variation is done symetrically between the outermost sites (site 1 & 5) with the second outer sites (site 2 & 4). Thus, we set $\epsilon_1 = \epsilon_5 = 3.4$ eV, $\epsilon_2 = \epsilon_4 = 0.3$ eV, and $\epsilon_3 = 0$. We see that the ϵ_i values with the best fit to the experimental data are roughly the same with the ratio we obtained before. These small difference may caused by several factors. One is a possible distorsion or asymmetry between the outermost sites and the second outer sites, as seen in Ref. [23], and the other one is an influence from the crystal environment. Contrary to the 3D model, the effects of U and V in this model are significant. Increases in either U or V will shift the loss function weight to larger photon energy. However without V, the loss function we get is very different from the experimental data.

This also suggests that the multiple plasmon peaks

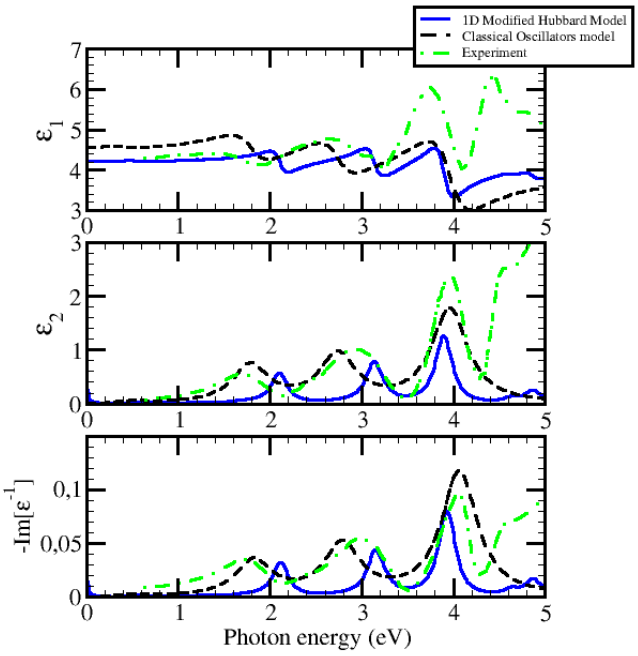

FIG. 2: ϵ_1 vs ω (top), ϵ_2 vs ω (middle), LF vs ω (bottom) for the finite-size 1D Hubbard model at nearly-quarter filling.

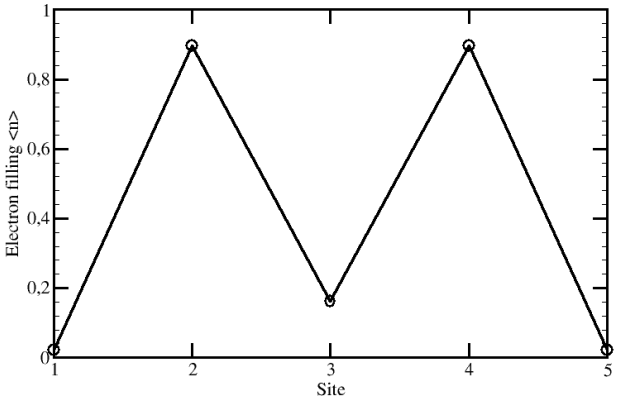

FIG. 3: Electron filling vs atomic sites.

in hp-SNO is only possible if we include the long-range Coulomb interactions. Shown in Fig. 2, there are three clear plasmon peaks of ϵ_2 and loss function at 2.12 eV, 3.17 eV, and 3.93 eV with amplitudes respectively from the first to the third peaks are around 0.03, 0.05, and 0.08. This resulting peaks are closely resemble the experimental loss function data of the $SrNbO_{3+\delta}$ film grown under high oxygen pressure [18].

In Fig.3, we demonstrate that electron confinement along with a not-so-large Hubbard-U induces strong cor-

relation effects that lead to a certain charges distribution in which excess of electrons resides in the nearest-neighbor of site with lack of electrons, confirming the picture of electron-hole pattern suggested in the classical coupled-oscillators model proposed in the previous study [18]. The high on-site energy at site 1 and 5 reduce the site occupation to nearly zero at the corresponding sites

The resulting density of state for 3D extended Hubbard model is shown in Fig. 4. Parameters used in this calculation are $t = 0.4$ eV, $U = 3.1$ eV, $V = 1.8$ eV, $a = 4.0$ Å, $\varepsilon(\infty) = 4$, and $n_{filling} = 0.2$. These parameters are choosen to be the same as the 1D Hubbard model so we can analyze the differences between the bulk and the confined system. Here we use ferromagnetic initial spin configurations as also used in [27]. It shows that since the chemical potential of the system located inside the band range, this system reveals metallic behavior(for full ferromagnetic ordering, band gap will appear if $U > 12t$). This result is also confirmed by the calculation of dielectric functions as shown in Fig. 5, which shows only a single conventional loss function peak at 1.9 eV.

In Fig. 5, we also show a coincidence of the plasmon peak with zero crossing of the real part of dielectric function which is similar with the experimental data obtained from $Sr_{1-x}NbO_{3+\delta}$ film grown under low oxygen pressure (lp-SNO) [18]. This similarity allows us to suspect that plasmons resonance occur on the lp-SNO system is caused by the conventional free charge oscillation with single oscillatory frequency as usually found in conventional metal. The insignificancy of U and V in the extended model is due to the electron filling that is far away from the half filling condition. Besides, the vanishing imaginary part of dielectric function and the small FWHM of loss function peak shown in the figure are also regarding to the weak correlation effects in our system.

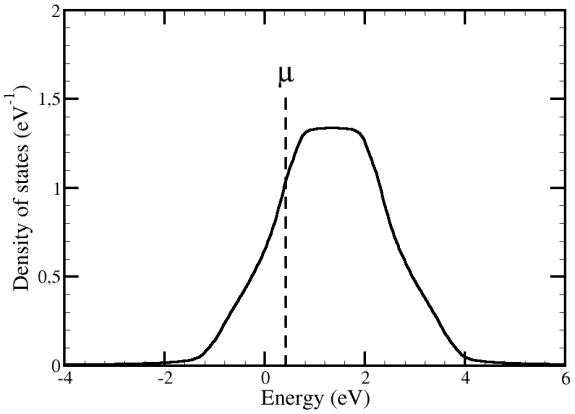

FIG. 4: DOS along with position of chemical potential μ at nearly zero temperature for the 3D Hubbard model , solved within self consistent mean-field approximation at nearly-quarter filling. The parameters used for the calculation is the same as the 1D Hubbard model. The chemical potential is located inside the band at 0.42 eV which indicates the bulk system is metallic.

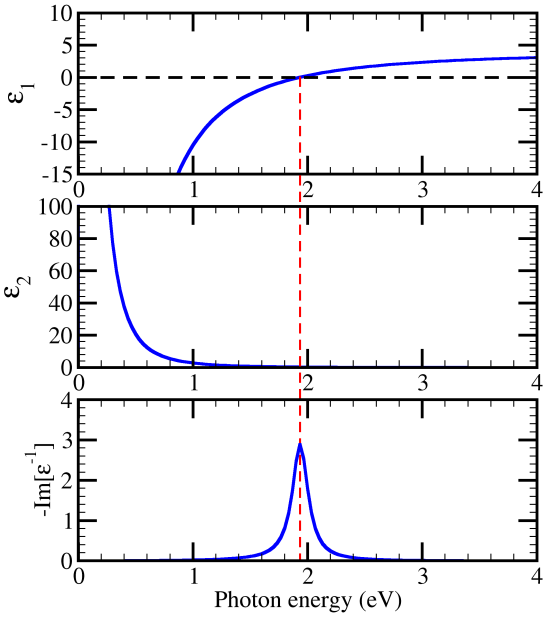

FIG. 5: ε_1 vs. ω (top), ε_2 vs. ω (middle), LF vs. ω (bottom) for the 3D Hubbard model at nearly-quarter filling. The loss function peak at 1.9 eV corresponds to the zero-crossing of ε_1 and vanishing ε_2, indicating that the plasmon is a conventional plasmon.

We have presented a theory explaining the mechanism of formation of unconventional plasmons in a weakly-correlated system such as $SrNbO_{3+\delta}$. In such system, extra oxygen planes confine the electrons in a quasi-one-dimensional nanometer scale, inducing strong correlation effects that transform the system from a metal into a Mott-like insulator, distribute the charges in an alternating pattern, and reveal the new kind of plasmons with unique characteristics different from those normally found in metals.

The authors thank Universitas Indonesia for funding this project through PITTA Research Grant No. 2285/UN2.R3.1/HKP.05.00/2018.

[1] J. D. Heber, Nature **461**, 720 (2009).
[2] J. A. Dionne and H. A. Atwater, MRS Bulletin **37**, 717724 (2012).
[3] P. West, S. Ishii, G. Naik, N. Emani, V. Shalaev, and A. Boltasseva, Laser & Photonics Reviews **4**, 795 (2010).
[4] J. A. Schuller, E. S. Barnard, W. Cai, Y. C. Jun, J. S. White, and M. L. Brongersma, Nature Materials **9**, 193

EP (2010), review Article.
[5] E. Ozbay, Science **311**, 189 (2006).
[6] S. A. Maier, *Plasmonics: Fundamentals and Applications* (Springer US, 2007).
[7] S. Lal, S. Link, and N. J. Halas, Nature Photonics **1**, 641 EP (2007), review Article.
[8] D. Bohm and D. Pines, Physical Review - PHYS REV X **82**, 625 (1951).
[9] D. Pines and D. Bohm, Phys. Rev. **85**, 338 (1952).
[10] D. Bohm and D. Pines, Phys. Rev. **92**, 609 (1953).
[11] R. H. Ritchie, Phys. Rev. **106**, 874 (1957).
[12] R. H. Ritchie, E. T. Arakawa, J. J. Cowan, and R. N. Hamm, Phys. Rev. Lett. **21**, 1530 (1968).
[13] K. Höflich, U. Gösele, and S. Christiansen, Phys. Rev. Lett. **103**, 087404 (2009).
[14] P. Kik and M. Brongersma, "Surface plasmon nanophotonics," (2007) pp. 1–9.
[15] E. Hutter and J. Fendler, Advanced Materials **16**, 1685 (2004).
[16] E. Petryayeva and U. J. Krull, Analytica Chimica Acta **706**, 8 (2011).
[17] E. G. C. P. van Loon, H. Hafermann, A. I. Lichtenstein, A. N. Rubtsov, and M. I. Katsnelson, Phys. Rev. Lett. **113**, 246407 (2014).
[18] T. C. Asmara, D. Wan, Y. Zhao, M. A. Majidi, C. T. Nelson, M. C. Scott, Y. Cai, B. Yan, D. Schmidt, M. Yang, T. Zhu, P. E. Trevisanutto, M. R. Motapothula, Y. P. Feng, M. B. H. Breese, M. Sherburne, M. Asta, A. Minor, T. Venkatesan, and A. Rusydi, Nature Communications **8**, 15271 EP (2017), article.
[19] T. Zhu, P. E. Trevisanutto, T. C. Asmara, L. Xu, Y. P. Feng, and A. Rusydi, Phys. Rev. B **98**, 235115 (2018).
[20] K. Persson, "Materials data on srnbo3 (sg:62) by materials project," (2015), an optional note.
[21] K. Persson, "Materials data on sr5nb5o17 (sg:58) by materials project," (2016), an optional note.
[22] C. Chen, S. Lv, Z. Wang, K. Akagi, F. Lichtenberg, Y. Ikuhara, and J. Georg Bednorz, Applied Physics Letters **105**, 221602 (2014).
[23] C. Chen, D. Yin, K. Inoue, F. Lichtenberg, X. Ma, Y. Ikuhara, and J. G. Bednorz, ACS Nano **11**, 12519 (2017).
[24] M. A. Majidi, H. Su, Y. P. Feng, M. Rübhausen, and A. Rusydi, Phys. Rev. B **84**, 075136 (2011).
[25] M. A. Majidi, E. Thoeng, P. K. Gogoi, F. Wendt, S. H. Wang, I. Santoso, T. C. Asmara, I. P. Handayani, P. H. M. van Loosdrecht, A. A. Nugroho, M. Rübhausen, and A. Rusydi, Phys. Rev. B **87**, 235135 (2013).
[26] M. A. Majidi, S. Siregar, and A. Rusydi, Phys. Rev. B **90**, 195442 (2014).
[27] D. Y. Wan, Y. L. Zhao, Y. Cai, T. C. Asmara, Z. Huang, J. Q. Chen, J. Hong, S. M. Yin, C. T. Nelson, M. R. Motapothula, B. X. Yan, D. Xiang, X. Chi, H. Zheng, W. Chen, R. Xu, Ariando, A. Rusydi, A. M. Minor, M. B. H. Breese, M. Sherburne, M. Asta, Q.-H. Xu, and T. Venkatesan, Nature Communications **8**, 15070 EP (2017), article.